

NEW HERA RESULTS ON DEEP-INELASTIC e^+p SCATTERING AT VERY HIGH Q^2

Ulrich F. Katz (ZEUS)

Physikalisches Institut, Universität Bonn

Nußallee 12, 53115 Bonn, Germany

Email: katz@physik.uni-bonn.de

Representing the H1 and ZEUS Collaborations

ABSTRACT

Until the end of 1997, the H1 and ZEUS experiments at the HERA collider at DESY both have collected an integrated luminosity of roughly 40 pb^{-1} of e^+p collisions. These data allow high-precision studies of deep-inelastic scattering of positrons on protons at large four-momentum transfer. Measurements of the differential cross-sections $d\sigma/dQ^2$ and $d\sigma/dx$ are reported and compared to predictions derived from measurements performed in fixed-target experiments at lower energies, extrapolated to the HERA kinematic regime using Standard Model calculations. In general, the HERA results agree well with the predictions. An excess of events at highest Q^2 in the 1994–1996 data, which was reported by both experiments, has not been corroborated by the new data but is still present in the combined data samples. Searches for signatures of production of positron-quark resonances or ($eeqq$) contact interactions have found no evidence for physics processes beyond the Standard Model, and new limits on the parameters of these scenarios are set.

1 Introduction

The electron^a–proton accelerator HERA at DESY in Hamburg, Germany, is providing ep collisions to the experiments H1¹ and ZEUS² since 1992. Between mid-1994 and the end of 1997 HERA has been operated with positrons (e^+) at an energy of $E_e = 27.5$ GeV and protons (p) of $E_p = 820$ GeV, yielding a center-of-mass energy of $\sqrt{s} = 300$ GeV. In this time, ZEUS and H1 have collected e^+p data samples corresponding to integrated luminosities of 46.6 pb^{-1} and 37.0 pb^{-1} , respectively. The analyses reported in this paper are based on these data, and are hence sensitive to processes with cross-sections as low as about 50 fb.

In the Standard Model (SM), deep-inelastic lepton–proton scattering proceeds to leading order via the two diagrams shown in Fig. 1, i.e. by the t -channel exchange of a γ or Z boson (neutral current, NC) or of a W boson (charged current, CC). Reaction products are the scattered lepton and a multi-particle hadronic system which evolves by fragmentation from the partonic final state and reflects its configuration in terms of energy flow and jet topology.

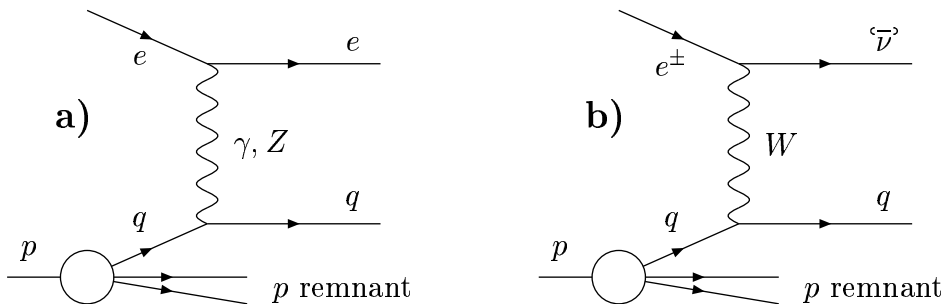


Figure 1: *Leading order Feynman graphs for deep-inelastic ep scattering (a) for NC and (b) for CC reactions. Note that scattering on antiquarks, produced in the proton by virtual processes, is also possible.*

For both reaction types, the relevant kinematic variables are given by

$$Q^2 = -q^2 = -(k - k')^2 \quad (1)$$

$$x = Q^2 / (2q \cdot P) \quad (2)$$

$$y = (q \cdot P) / (k \cdot P) , \quad (3)$$

^a Here and in the following, the term *electron* will denote both electrons and positrons, unless explicitly stated otherwise.

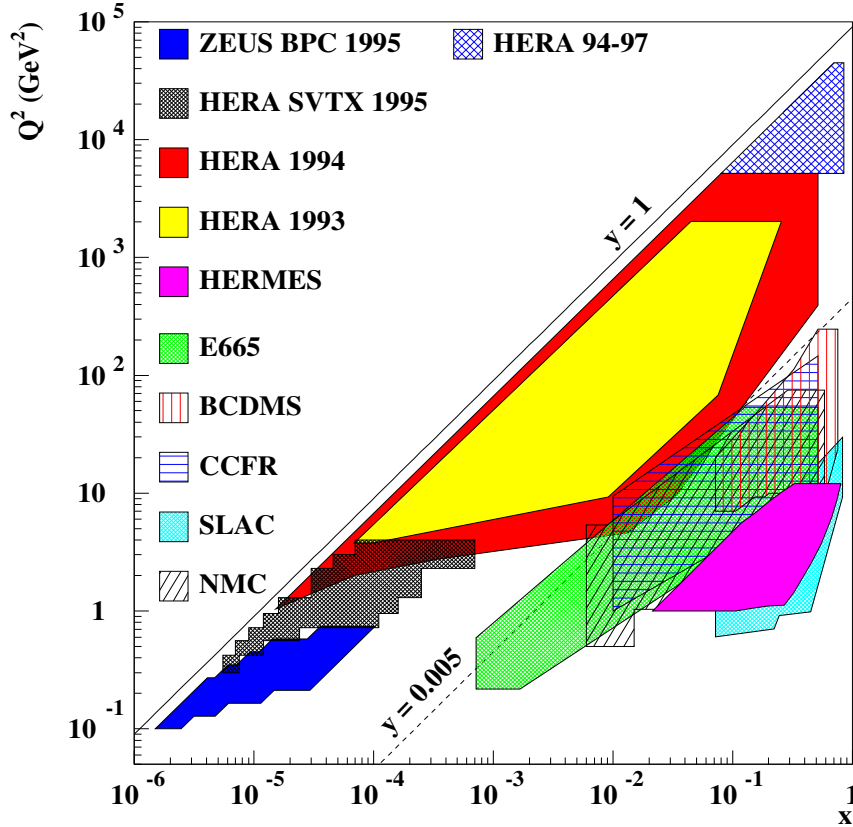


Figure 2: *Regions in the HERA kinematic (x, Q^2) -plane covered by structure function and cross-section measurements of ZEUS and H1 and of the fixed-target experiments with charged lepton beams (BCDMS, NMC, E665, SLAC) and with neutrino beams (CCFR).*

where k , k' and P are the four-momenta of the initial and the final-state lepton^b and of the incoming proton, respectively (see Fig. 1). Q^2 measures the virtuality of the gauge boson and reaches values of above 10^4 GeV^2 at HERA, corresponding to a spatial resolution of $\mathcal{O}(10^{-16} \text{ cm})$ with which structures in the proton can be resolved. The Bjorken scaling variable x indicates the fraction of the proton momentum carried by the struck quark, and y is related to the eq center-of-mass scattering angle θ^* by $y = (1 - \cos\theta^*)/2$ (where $\theta^* = 0$ for forward scattering). For $k_\gamma = 0$, these variables are related by $Q^2 = x \cdot y \cdot s$. The invariant mass of the electron-quark system is given by $M = \sqrt{xs}$.

The kinematic regime covered by the HERA and the fixed-target experiments is indicated in Fig. 2. This report will focus on Q^2 values exceeding a few 100 GeV^2 ,

^b If a photon with four-momentum k_γ is radiated off the initial or final-state lepton, q has to be replaced by $q = k - k' - k_\gamma$ in eqs. (1-3).

and in particular on the region of highest Q^2 indicated by the cross-hatched region, where the differential cross-sections are small and where detailed studies only have become possible with the high-statistics data collected in 1996 and 1997. The high- Q^2 event topologies are shown in Fig. 3. Note that for Q^2 above $\mathcal{O}(1000 \text{ GeV}^2)$ the scattered electron is deflected under large angles w.r.t. its original direction and has energies up to several 100 GeV.

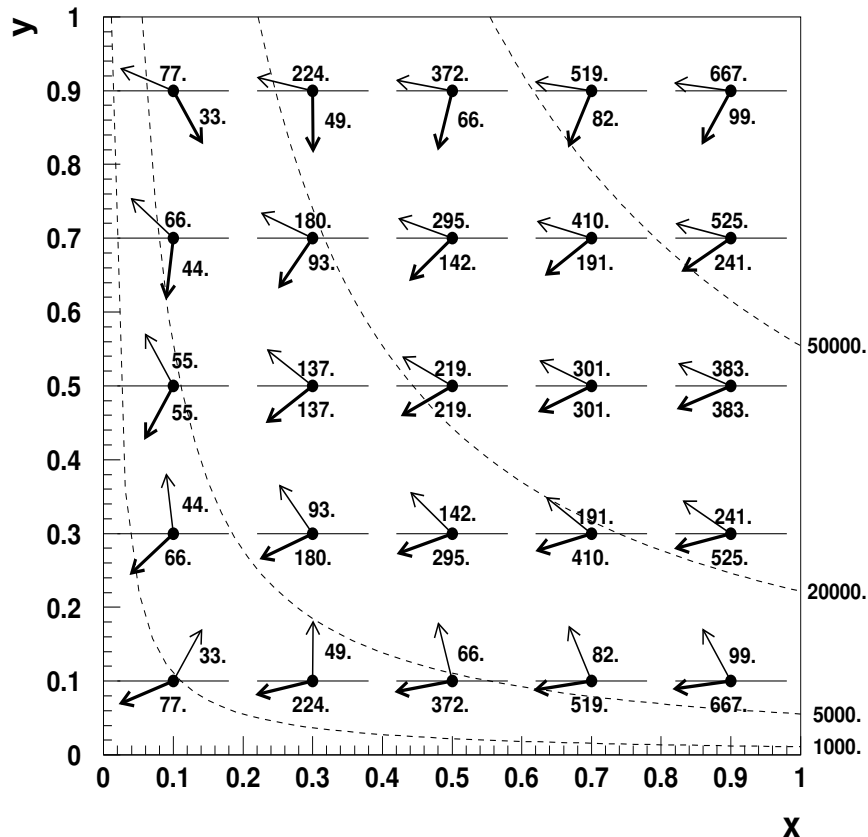


Figure 3: *Event topologies for different values of x and y , in the absence of QED radiation (i.e. $k_\gamma = 0$). Each event pictogram shows the directions in which lepton (upper arrow) and quark (lower arrow) are emitted in reactions with x and y being given by the position of the central dot. Quasi-free, massless quarks have been assumed for relating x and y with the scattering angles. The numbers next to the arrows represent the electron and quark energies in GeV. The dashed lines indicate constant values of Q^2 (in GeV^2).*

Particular interest in DIS at highest Q^2 was stimulated when both the ZEUS³ and the H1⁴ collaborations reported an excess of NC events over the SM expectation at $Q^2 \gtrsim 2 \cdot 10^4 \text{ GeV}^2$ in their 1994–1996 data. Figure 4 shows the NC cross-section as a function of a lower cutoff in Q^2 as measured by ZEUS and H1 using the data taken until mid-1997. Several scenarios beyond the SM have been suggested to

account for this high- Q^2 excess. The main objective of this report is to summarize the latest developments of cross-section measurements and searches for new physics in the high- Q^2 e^+p DIS data taken at HERA.

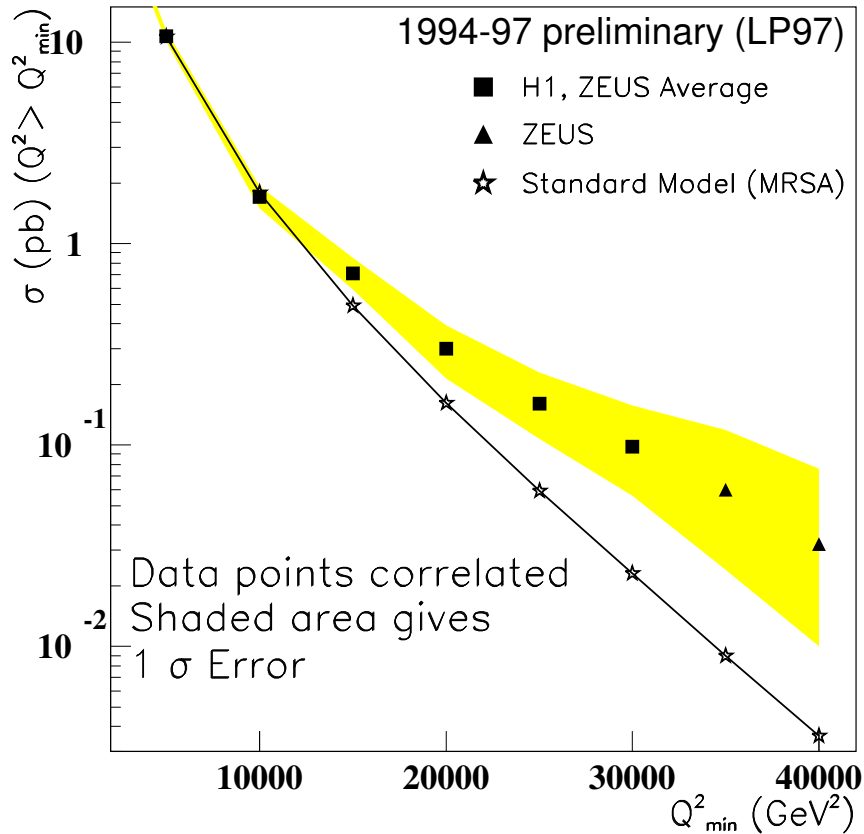


Figure 4: NC cross sections for $Q^2 > Q_{\min}^2$ with $Q_{\min}^2 > 5000 \text{ GeV}^2$. Shown are the combined ZEUS and H1 results (squares) and the corresponding one-sigma error band (shaded region). Note that the triangles in the domain $Q^2 \geq 35000 \text{ GeV}^2$ are the ZEUS cross-sections and contain no averaging with the zero events observed by H1 in this region.

After a short synopsis of experimental issues (section 2), we summarize some essential formulae describing the DIS cross-sections in the SM (section 3), review new NC and CC cross-section measurements at high Q^2 reported recently by ZEUS^{5,6} and H1⁷ (section 4) and finally report on searches for resonance production^{8,9} and contact interactions^{10,11} in the high- Q^2 DIS data (section 5). A short summary and outlook concludes this report (section 6). A review of QCD analyses based on the HERA data which also refers to the high- Q^2 cross-sections can be found in a separate contribution to these proceedings.¹²

2 Experimental Issues

The calorimeters are the principal components for both the ZEUS and the H1 high- Q^2 analyses. ZEUS uses a compensating uranium-scintillator sandwich calorimeter with energy resolutions of $\Delta E/E = 18\%/\sqrt{E} [\text{GeV}]$ for electrons and $\Delta E/E = 35\%/\sqrt{E} [\text{GeV}]$ for hadrons (under test beam conditions). H1 employs a liquid-argon (LAr) calorimeter covering the central and forward^c region, and a lead scintillating-fiber calorimeter in the rear direction. The LAr resolutions (relevant for high- Q^2 analyses) are $\Delta E/E = 12\%/\sqrt{E} [\text{GeV}]$ for electrons and $\Delta E/E = 50\%/\sqrt{E} [\text{GeV}]$ for hadrons. The absolute energy scales are known to a precision of about 1.5% (electrons) and 3 – 4% (hadrons) in both experiments. Momenta of charged particles and event vertices are reconstructed using the central tracking devices which are complemented by forward and rear planar chambers and operate in a longitudinal magnetic field (1.43 T in ZEUS, 1.15 T in H1).

In both experiments the luminosity is measured to a precision of about 1.5% using external electromagnetic calorimeters placed down-stream in e -beam direction which are designed to measure the rates of electrons and photons from Bethe-Heitler processes ($ep \rightarrow ep\gamma$).

A schematic overview over the general detector layout of both experiments, together with typical high- Q^2 event signatures, is shown in Fig. 2.

The trigger decision for NC candidates is based mainly on energies deposited in the calorimeter, specifically on the electromagnetic energy and on various energy sums like the total transverse energy (E_t). For CC events the net transverse momentum constitutes the main signature.

In the offline event reconstruction an algorithm is applied to identify scattered electrons using the topology of their calorimeter signal and the tracking information. NC events are identified mainly by the presence of an isolated electron candidate with energy above typically 10 GeV, and by longitudinal energy-momentum containment. The kinematic variables for NC candidate events are calculated either from the scattering angle of the electron and an overall hadronic angle (double-angle method, ZEUS), or from a combination of energy and angle of the scattered

^c Both experiments define their Z axis parallel to the proton beam direction, with the nominal interaction point being the coordinate system origin. The polar angle, θ , and the forward and rear directions are defined w.r.t. the Z axis. The pseudorapidity is given by $\eta = -\ln \tan(\theta/2)$.

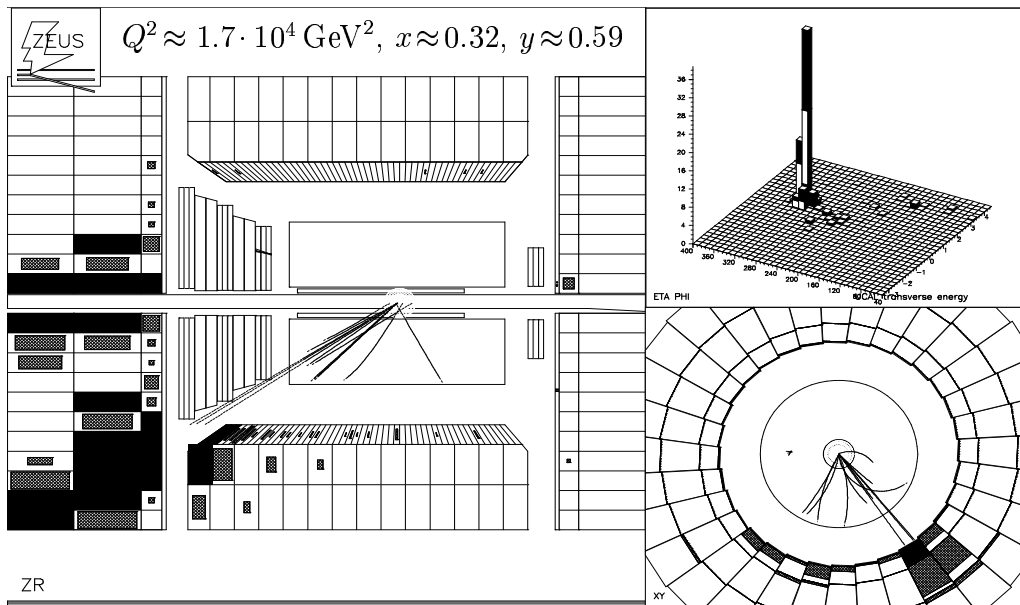
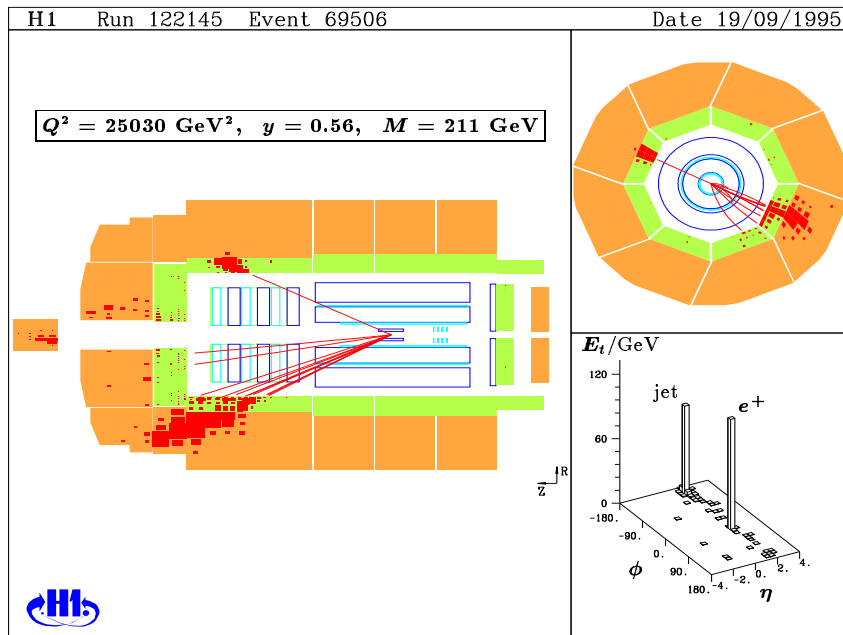


Figure 5: Event displays of high- Q^2 e^+p reactions: A NC event in the H1 detector (top) and a CC event in ZEUS (bottom). The left parts of both pictures show vertical cuts through the detectors along the beam direction, with the positron entering from the left and the proton from the right. The tracks reconstructed from the hits in the inner tracking chambers and the energy deposits in the surrounding calorimeters are indicated. The two smaller displays at the right show transverse cuts through the central detectors and the flow of transverse energy in the pseudorapidity–azimuth plane, respectively. The reconstructed kinematic variables of each event are indicated on top of the displays.

electron and hadronic variables ($e\Sigma$ -method, H1). The resolutions of x , y and Q^2 for NC events are typically of $\mathcal{O}(5\%)$ and generally better than 10%.

CC events are selected requiring a net transverse momentum above a threshold and the absence of a scattered electron. The kinematic variables have to be determined from hadronic measurements only, resulting in resolutions of about 15% – 25% except at very high y , where they are worse.

3 DIS in the Standard Model

In the naïve quark-parton model (QPM), e^+p DIS proceeds via lepton-quark scattering according to the Feynman graphs shown in Fig. 1, where the quark is assumed to be quasi-free, massless, and collinear with the incoming proton. In this picture the DIS cross-section is given by the $e\bar{q}$ matrix elements (which are fully calculable within the SM) and the probability densities $q(x)$ ($\bar{q}(x)$) to find a quark q (antiquark \bar{q}) of a given flavor in the proton which carries a fraction x of its momentum. The effects of the strong interaction can be taken into account by applying the QCD-based DGLAP evolution prescription¹³ to the parton density functions (PDF's) which thereby acquire an effective Q^2 dependence.

The NC cross-section incorporating leading-order QCD corrections is given by

$$\frac{d^2\sigma^{e^\pm p \rightarrow e^\pm X}}{dx dQ^2}(x, Q^2) = \frac{2\pi\alpha^2}{Q^4} \left[(1 + (1-y)^2) \mathcal{F}_2^{\text{NC}} \mp (1 - (1-y)^2) \mathcal{F}_3^{\text{NC}} \right] \quad (4)$$

$$\mathcal{F}_2^{\text{NC}}(x, Q^2) = \sum_{q=d,u,s,c,b} A_q(Q^2) \cdot [q(x, Q^2) + \bar{q}(x, Q^2)] \quad (5)$$

$$\mathcal{F}_3^{\text{NC}}(x, Q^2) = \sum_{q=d,u,s,c,b} B_q(Q^2) \cdot [q(x, Q^2) - \bar{q}(x, Q^2)] \quad (6)$$

$$A_q(Q^2) = \frac{1}{2} [(V_L^q)^2 + (V_R^q)^2 + (A_L^q)^2 + (A_R^q)^2] \quad (7)$$

$$B_q(Q^2) = [(V_L^q)(A_L^q) - (V_R^q)(A_R^q)] \quad (8)$$

with

$$\begin{aligned} V_{L,R}^q &= Q_q - (v_e \pm a_e) v_q P_Z \\ A_{L,R}^q &= - (v_e \pm a_e) a_q P_Z \\ v_f &= \frac{I_f^3 - 2 \sin^2 \theta_w Q_f}{2 \sin \theta_w \cos \theta_w}, \quad a_f = \frac{I_f^3}{2 \sin \theta_w \cos \theta_w} \\ P_Z &= \frac{Q^2}{Q^2 + M_Z^2}. \end{aligned} \quad (9)$$

In eq. (9), the plus sign applies to the left-handed coefficients (index L), v_f and a_f are the SM vector and axial-vector coupling constants of a fermion f , Q_f and I_f^3 denote its charge and third component of the weak isospin, and M_Z and θ_w are the Z mass and the Weinberg angle. The top quark contribution to the NC ep cross-section is completely suppressed at HERA energies.

For CC scattering, the corresponding cross-section is

$$\frac{d^2\sigma^{e^\pm p \rightarrow \vec{\nu} X}}{dx dQ^2} = \frac{\pi\alpha^2}{8\sin^4\theta_w Q^4} \left[(1 + (1-y)^2) \mathcal{F}_2^{\text{CC}\pm} \mp (1 - (1-y)^2) \mathcal{F}_3^{\text{CC}\pm} \right] \quad (10)$$

$$\mathcal{F}_{2,3}^{\text{CC}+} = \left(\frac{Q^2}{Q^2 + M_W^2} \right)^2 \cdot \left[\sum_{q=d,s} q(x, Q^2) \pm \sum_{q=u,c} \bar{q}(x, Q^2) \right] \quad (11)$$

$$\mathcal{F}_{2,3}^{\text{CC}-} = \left(\frac{Q^2}{Q^2 + M_W^2} \right)^2 \cdot \left[\sum_{q=u,c} q(x, Q^2) \pm \sum_{q=d,s} \bar{q}(x, Q^2) \right] \quad (12)$$

with M_W being the W mass. Note that electrons and positrons couple to quarks and antiquarks of different flavor, as required by charge conservation: $Q_e + Q_q = Q_{q'}$. Quark mass effects are neglected in eqs. (11) and (12). The tiny contributions of bottom and top quarks to the cross-section are ignored.

In order to evaluate the above cross-sections, two sets of ingredients are needed: the electroweak parameters like $\sin^2\theta_w$, M_Z etc., which are known to high precision from the e^+e^- experiments at LEP and SLAC, and the PDF's. The latter have been parameterized by several theory groups (see e.g. ref. 14–16) using fits to the relevant data (mainly measurements of DIS structure functions and cross-sections) in which the next-to-leading order QCD evolution is imposed. A typical set of PDF's is shown in Fig. 6. It becomes obvious that at $x \gtrsim 0.1$ the valence quark distributions (i.e. $q_v \equiv q - \bar{q}$) are dominant, and also that the d/u ratio falls far below the naïve expectation of 0.5 at high x .

From eqs. (4-9) it can be seen that at $Q^2 \ll M_Z^2$, the NC cross-section is dominated by the photon exchange, and the five “light” quark flavors contribute in proportion to their charge squares. In particular, u and d enter in the combination $4u + d$. For higher Q^2 , this relation becomes y -dependent, but the u contribution remains to be the largest one. For CC scattering, (see eqs. (4-12)) $e^+(e^-)$ beams “see” d -type quarks and u -type antiquarks (u -type quarks and d -type antiquarks). In particular, e^+p CC scattering at high x is dominated by the d distribution. For $Q^2 \gtrsim M_W^2, M_Z^2$ the contributions of Z and W exchange

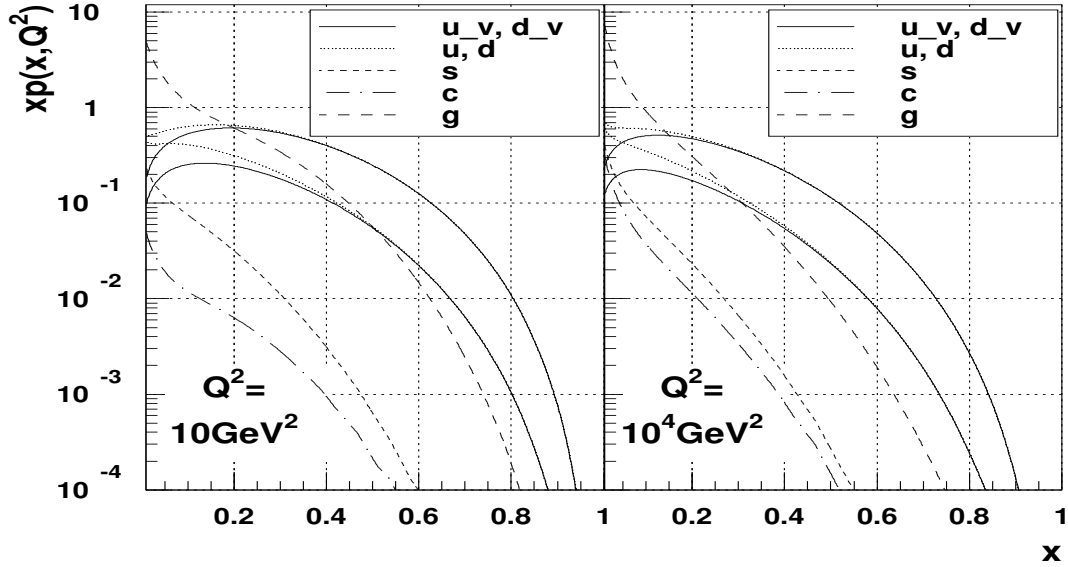


Figure 6: PDF's for $Q^2 = 10 \text{ GeV}^2$ (left) and for $Q^2 = 10^4 \text{ GeV}^2$ (right). The larger of the two valence distributions represents u_v , the differences between the dotted and the solid lines indicate the u and d sea quark distributions.

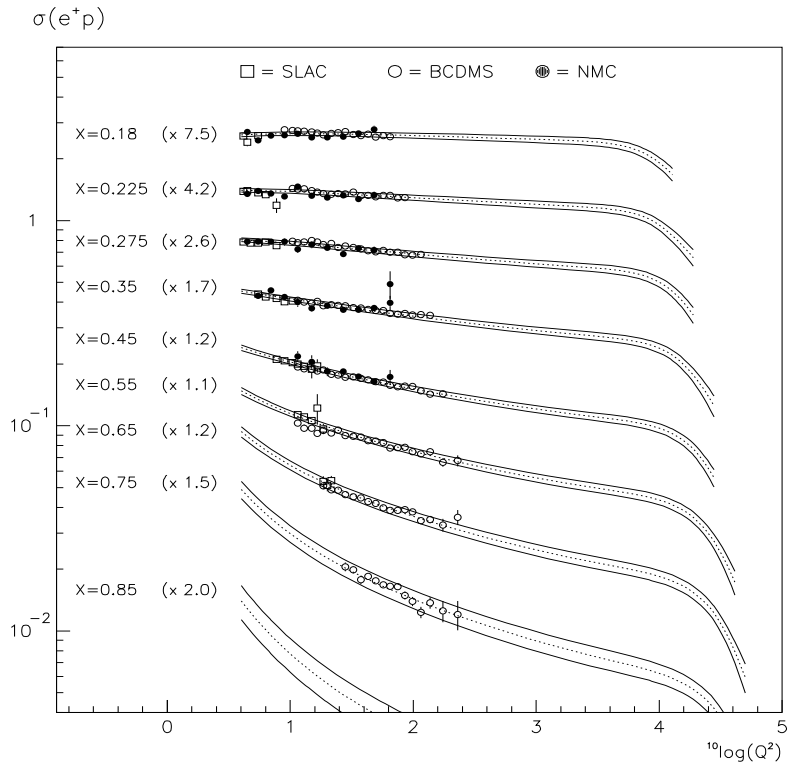


Figure 7: Reduced e^+p cross-sections for NC scattering from the PDF fit by M.Botje (ZEUS). The error bands indicate the overall cross-section uncertainties resulting from propagating the errors on the input data and on α_s through the fit procedure.

to the DIS cross-sections become of similar magnitude as that of the photon exchange. The HERA experiments are the first having the possibility to observe this manifestation of electroweak unification in the space-like regime.

The uncertainties of the cross-sections calculated from eqs. (4) and (10) (or rather from their equivalents incorporating the next-to-leading order QCD corrections and the full one-loop electroweak corrections) are dominated by the PDF's, more specifically by the experimental errors of the input data to the PDF fits, and by theoretical uncertainties related to higher-order corrections, to the treatment of the heavy quark PDF's, and to the value of α_s . In order to obtain a realistic PDF error estimate, M.Botje from the ZEUS collaboration has performed a QCD fit¹⁷ to the relevant fixed-target data and propagated the sources of uncertainties into errors on the reduced NC cross-section,

$$\tilde{\sigma}^{e^\pm p \rightarrow e^\pm X}(x, Q^2) = \frac{xQ^4}{2\pi\alpha^2(1+(1-y)^2)} \cdot \frac{d^2\sigma^{\text{NC}}}{dx dQ^2} \quad (13)$$

(see Fig. 7). The resulting overall cross-section uncertainty amounts to about $\pm 7\%$ at high x and Q^2 . A similar study for e^+p CC reactions yielded larger uncertainties which rapidly grow with Q^2 and exceed 20% for $Q^2 \gtrsim 2 \cdot 10^4 \text{ GeV}^2$ or $x \gtrsim 0.5$.

4 Cross-Section Measurements

Both ZEUS^{5,6} and H1⁷ reported new preliminary cross-section measurements for high- Q^2 NC and CC DIS at the ICHEP98 conference in Vancouver. These analyses are based on the full e^+p data sets collected until end of 1997 (integrated luminosities of 46.6 pb^{-1} for ZEUS and 37.0 pb^{-1} for H1), and include substantial improvements of data statistics, detector calibration, analysis methods, and Monte Carlo simulation as compared to the status of summer 1997.¹⁸

NC Cross-Sections:

For the NC analyses, ZEUS considers reactions with $Q^2 > 400 \text{ GeV}^2$ and $y_e < 0.95$ (y_e being the value of y as reconstructed from the measured momentum of the scattered electron). H1 applies the cuts $Q^2 > 200 \text{ GeV}^2$ and $y_e < 0.9$. The final event samples consist of 38000 events (ZEUS) and 75000 events (H1).

On the next pages, the latest HERA NC e^+p cross-section measurements are presented: $d\sigma/dQ^2$ from ZEUS (Fig. 8) and H1 (Fig. 9), $d\sigma/dx$ from ZEUS (Fig. 10)

ZEUS NC Preliminary 1994 – 97

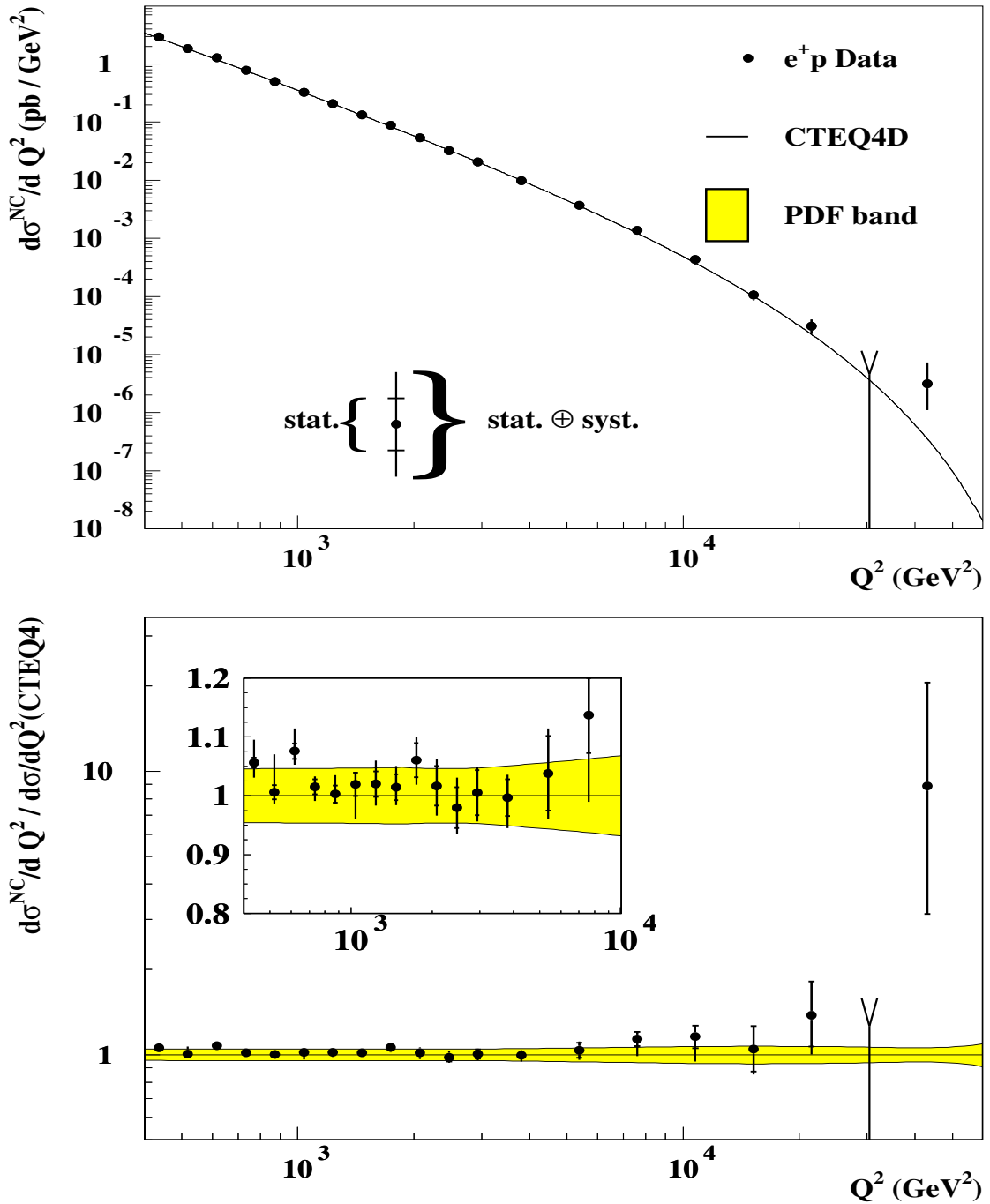


Figure 8: In the top plot, the points with error bars indicate the ZEUS results for the radiatively corrected differential NC e^+p cross-section $d\sigma/dQ^2$. The line is the theoretical prediction, calculated by integrating eq. (4) over x . The bottom plot shows the ratio of measured to expected cross-sections, with the shaded band indicating the PDF uncertainty (see Fig. 7).

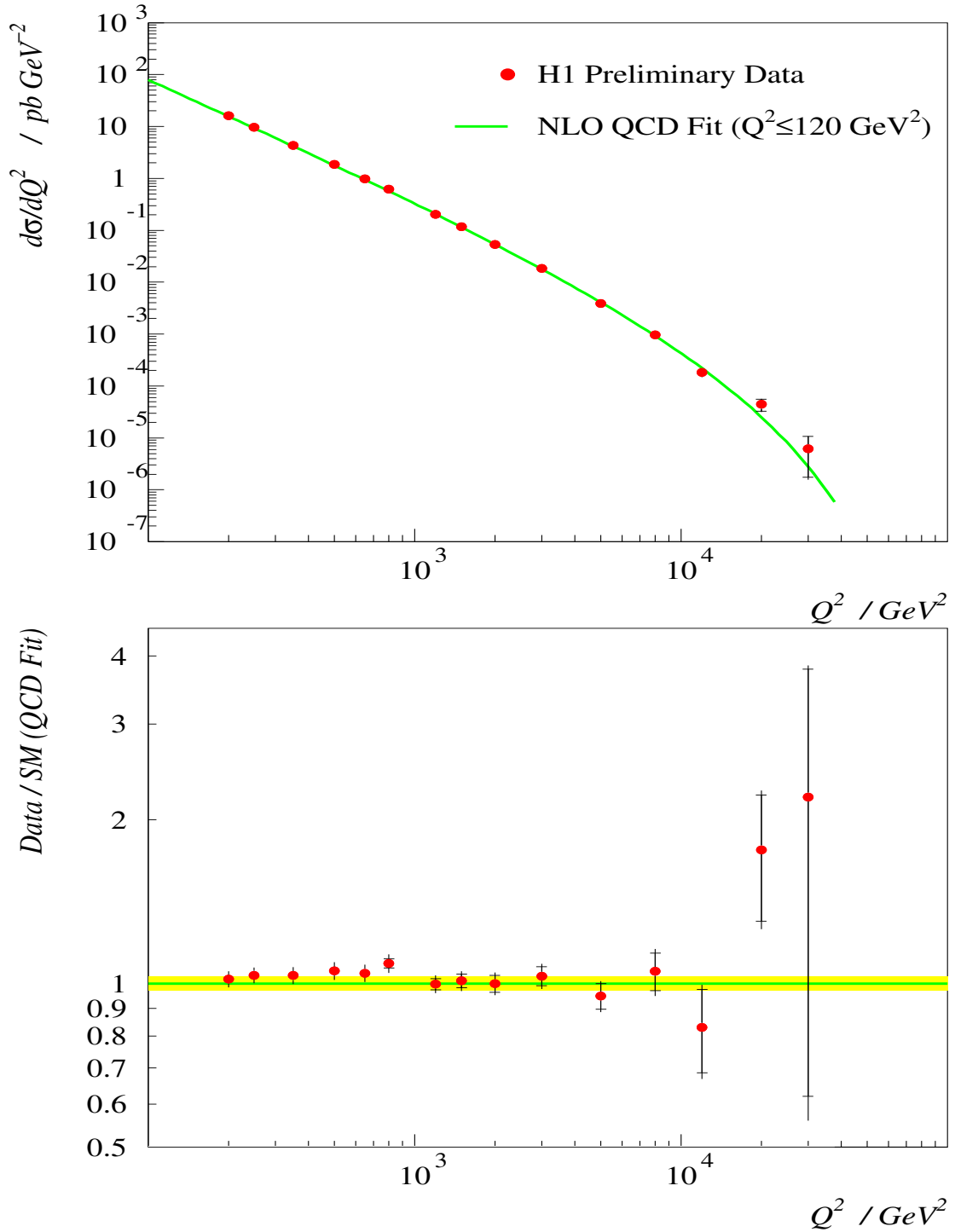


Figure 9: In the top plot, the points with error bars indicate the H1 results for the radiatively corrected differential NC e^+p cross-section $d\sigma/dQ^2$. The line is the theoretical prediction, calculated by integrating eq. (4) over x . The bottom plot shows the ratio of measured to expected cross-sections, with the shaded band indicating the H1 luminosity uncertainty.

ZEUS NC Preliminary 1994 – 97

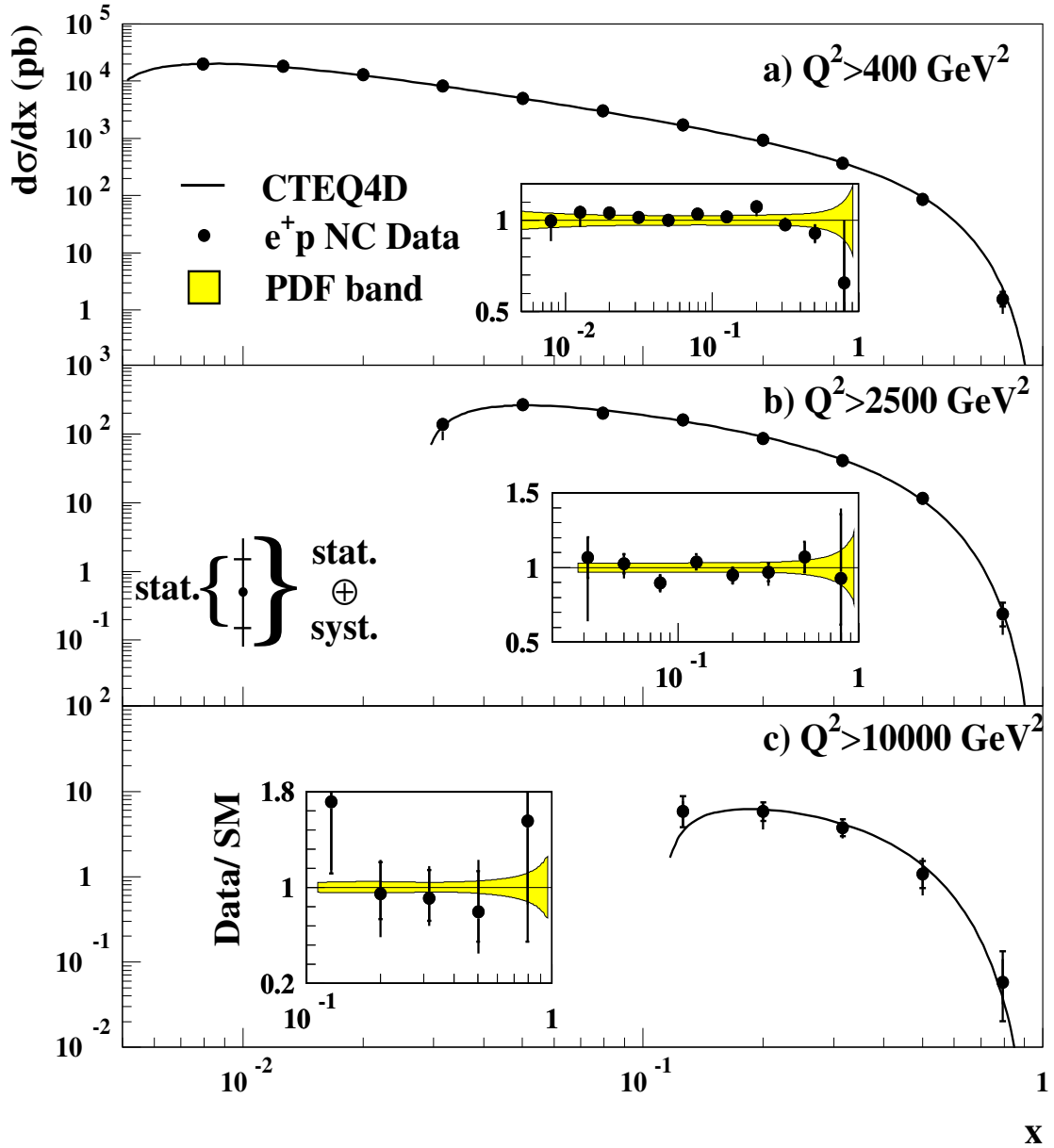


Figure 10: Radiatively corrected differential NC e^+p cross-section $d\sigma/dx$ as measured by ZEUS, for three different lower Q^2 -cutoffs. The points with error bars are the experimental results, the lines show the theoretical predictions. The insert plots show the ratio of measured to expected cross-sections, with the shaded band indicating the PDF uncertainty (see Fig. 7).

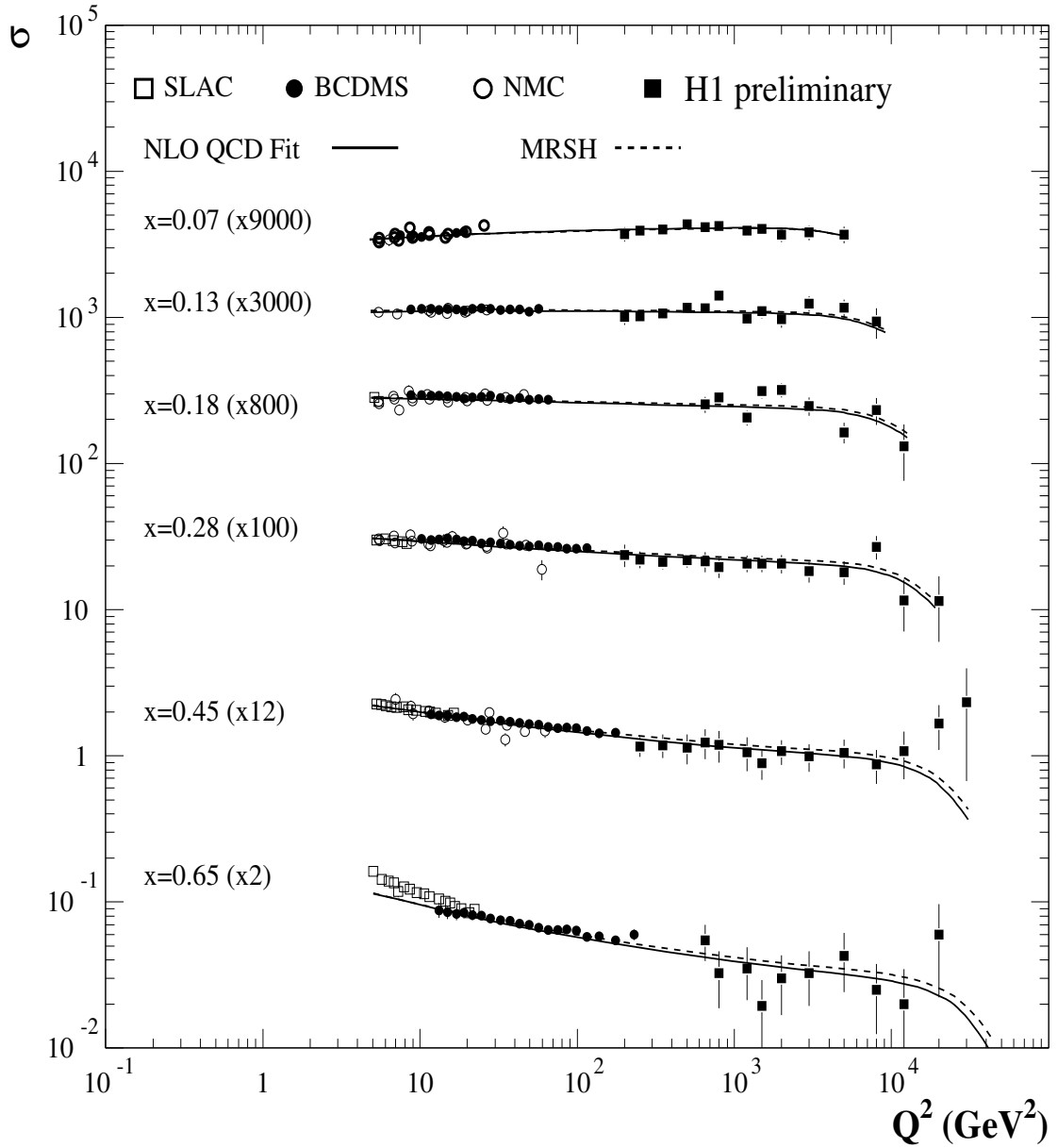


Figure 11: Radiatively corrected reduced NC e^+p cross-section $\tilde{\sigma}(x, Q^2)$ as measured by H1, as a function of Q^2 for different fixed values of x (big dots with error bars). Also indicated are corresponding results of fixed-target experiments (small symbols). The lines indicate the theoretical predictions, derived (i) from the PDF set MRSH¹⁹ (dashed), and (ii) from a QCD-fit performed by the H1 collaboration (solid).

and the reduced cross-section $\tilde{\sigma}(x, Q^2)$ from H1 (Fig. 11). The cross-sections are radiatively corrected to the Born-level. The systematic errors are added in quadrature to the statistical ones and are mainly caused by uncertainties of the energy scale calibration^d, the detector simulation, the trigger and vertex-reconstruction efficiencies, and the luminosity measurement. None of these sources is dominant, and the combined systematic uncertainties amount to a few percent. For $Q^2 \gtrsim 1000 \text{ GeV}^2$, the precision of the analyses is statistics-limited.

In general, very good agreement is observed between measured and expected cross-sections. Possible exceptions are the region $Q^2 \gtrsim 20000 \text{ GeV}^2$, where both ZEUS and H1 observe a higher cross-section than expected (see Figs. 8 and 9), and the x -interval around $x = 0.45$, where the reduced cross-section of H1 (Fig. 11) is above the expectation^e. No anomaly around $x = 0.45$ is apparent in the ZEUS data of Fig. 10. Clearly, these observations are related to the high- Q^2 excess reported in refs. 3 and 4. Without further discussion, we quote the relevant event numbers: for $Q^2 > 35000 \text{ GeV}^2$, ZEUS observes 2 events and expects 0.29 ± 0.02 (was 2 events vs. 0.15 ± 0.01 expected in 1994–96 data). For $|M - 200 \text{ GeV}| < 12.5 \text{ GeV}$ (corresponding to $0.39 < x < 0.50$), H1 now observes 8 events and expects 3.0 ± 0.5 (was 7 events vs. 0.95 ± 0.18 expected in the 1994–96 data).

CC Cross-Sections:

For the measurements of the CC cross-sections ZEUS uses the event sample with $p_t > 10 \text{ GeV}$ (p_t being the net transverse momentum of the event), $Q^2 > 400 \text{ GeV}$ and $y < 0.9$ (altogether 869 events). H1 requires $p_t > 12 \text{ GeV}$, $x > 0.01$ and $y < 0.9$ (656 events). For both experiments, the systematic uncertainty of the cross-section measurement is dominated by the hadronic energy scale uncertainty.

On the following pages, the differential cross-sections $d\sigma/dQ^2$ from H1 (Fig. 12) and ZEUS (Fig. 13) as well as $d\sigma/dx$ (Fig. 14) and $d\sigma/dy$ (Fig. 15) from ZEUS are shown. Again, there seems to be a weak indication for an excess of measured over expected cross-sections at highest Q^2 (see Figs. 12 and 13) and highest x (Fig. 14).

^d This affects H1 more than ZEUS who use the energy-scale independent double-angle method, which in turn suffers from systematic effects related to the hadronic measurements.

^e Note that the statistical errors in the cross-section plots are calculated from the numbers of observed events and are therefore not suited to assess the significance of a possible excess, which has to be evaluated using confidence intervals based on the numbers of expected events.

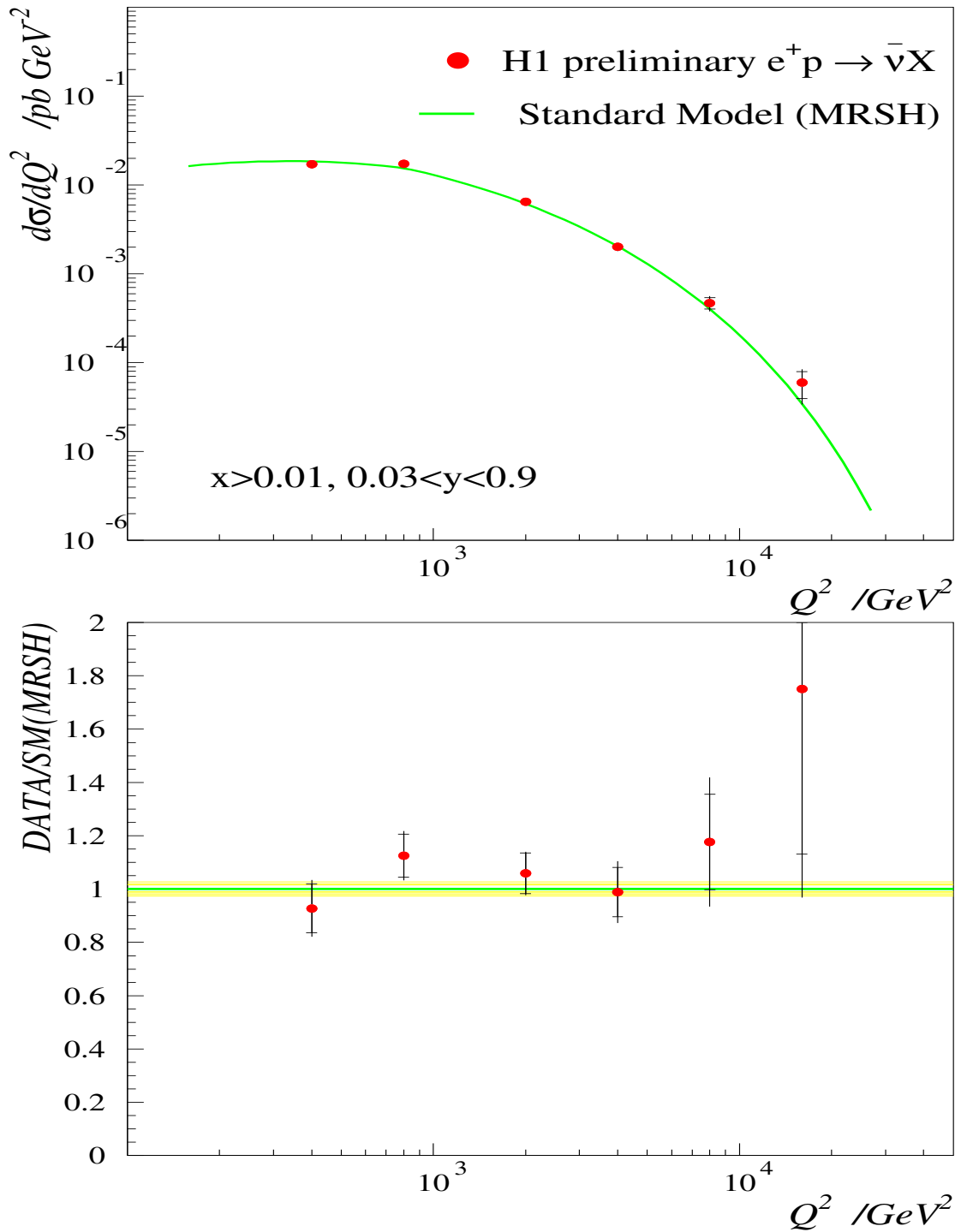


Figure 12: In the top plot, the points with error bars indicate the H1 results for the radiatively corrected differential CC e^+p cross-section $d\sigma/dQ^2$, restricted to the kinematic region $x > 0.01$ and $y < 0.9$. The line is the theoretical prediction, calculated by integrating eq. (10) over x . The bottom plot shows the ratio of measured to expected cross-sections, with the shaded band indicating the H1 luminosity uncertainty.

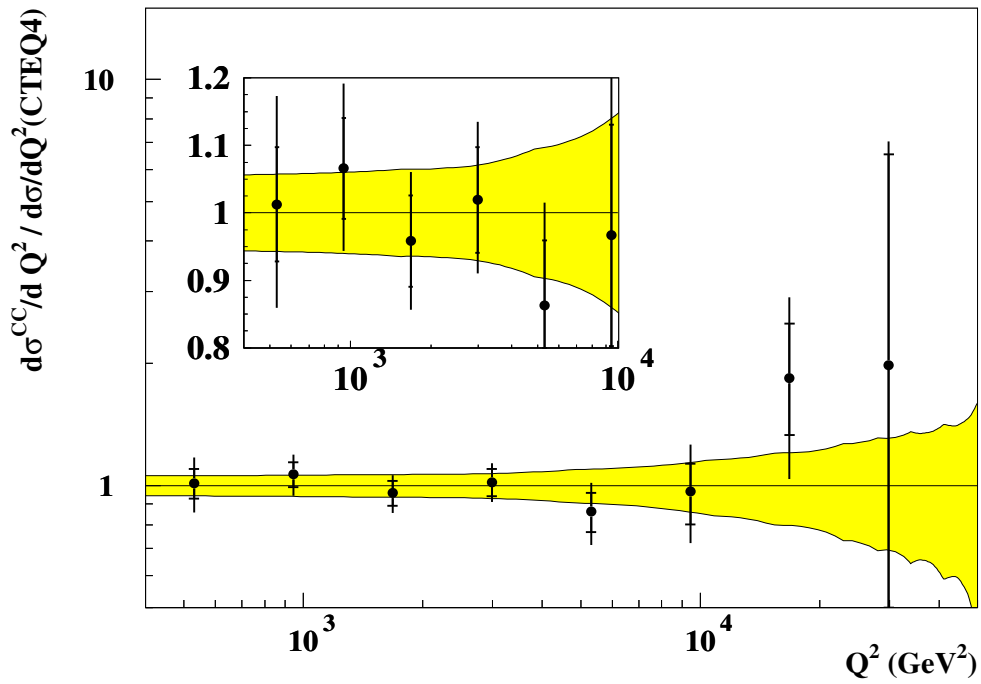
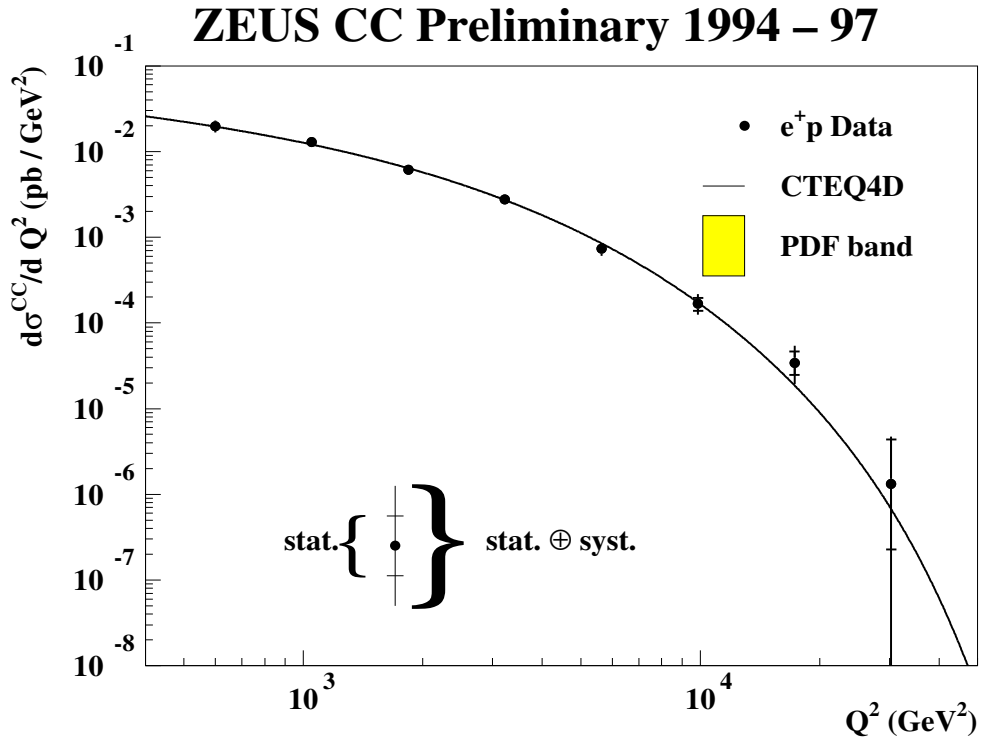


Figure 13: In the top plot, the points with error bars indicate the ZEUS results for the radiatively corrected differential CC e^+p cross-section $d\sigma/dQ^2$. The line is the theoretical prediction, calculated by integrating eq. (10) over x . The bottom plot shows the ratio of measured to expected cross-sections, with the shaded band indicating the PDF uncertainty.

ZEUS CC Preliminary 1994-97

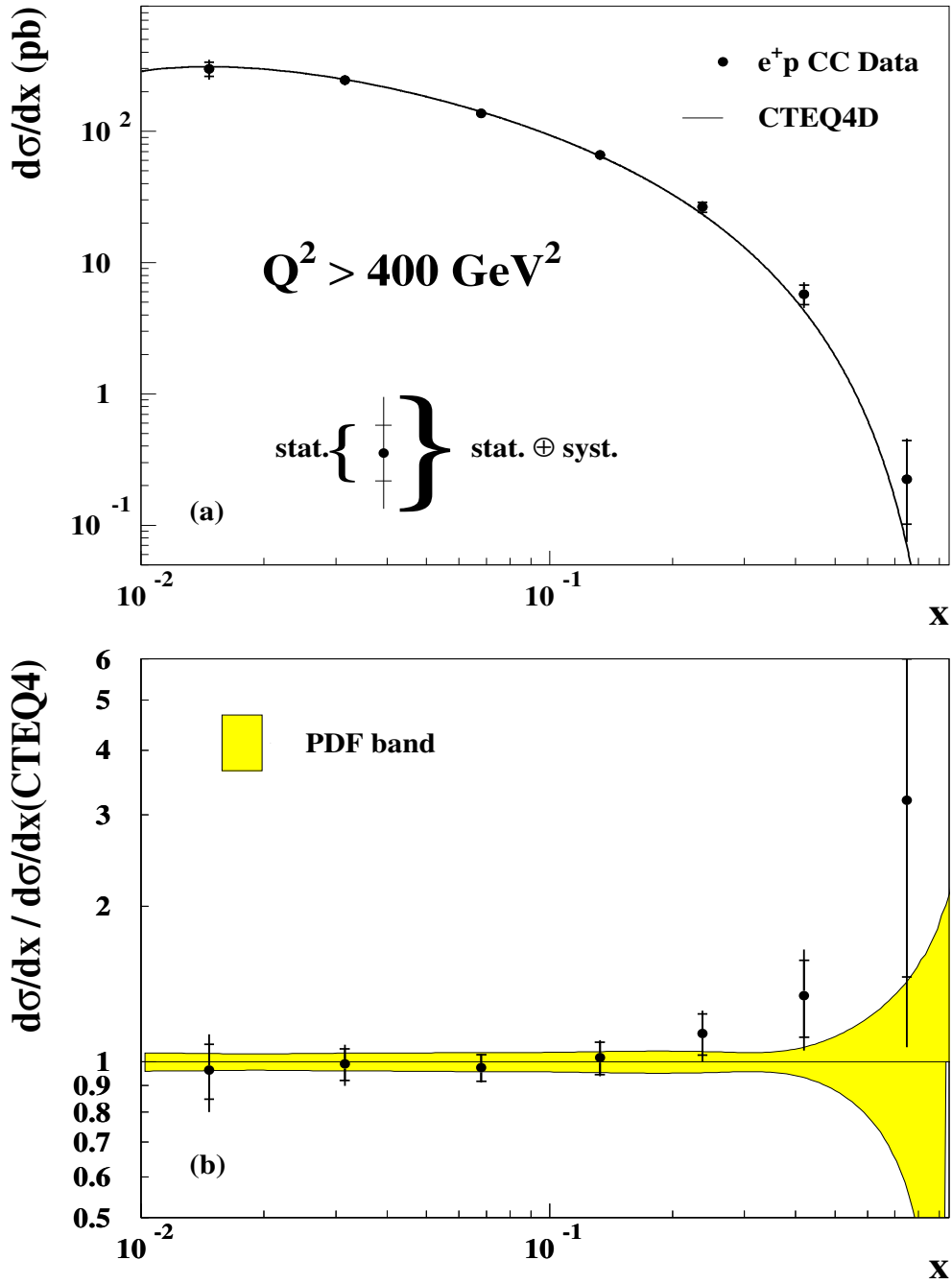


Figure 14: In the top plot, the points with error bars indicate the ZEUS results for the radiatively corrected differential CC e^+p cross-section $d\sigma/dx$. The line is the theoretical prediction, calculated by integrating eq. (10) over Q^2 . The bottom plot shows the ratio of measured to expected cross-sections, with the shaded band indicating the PDF uncertainty.

ZEUS CC Preliminary 1994-97

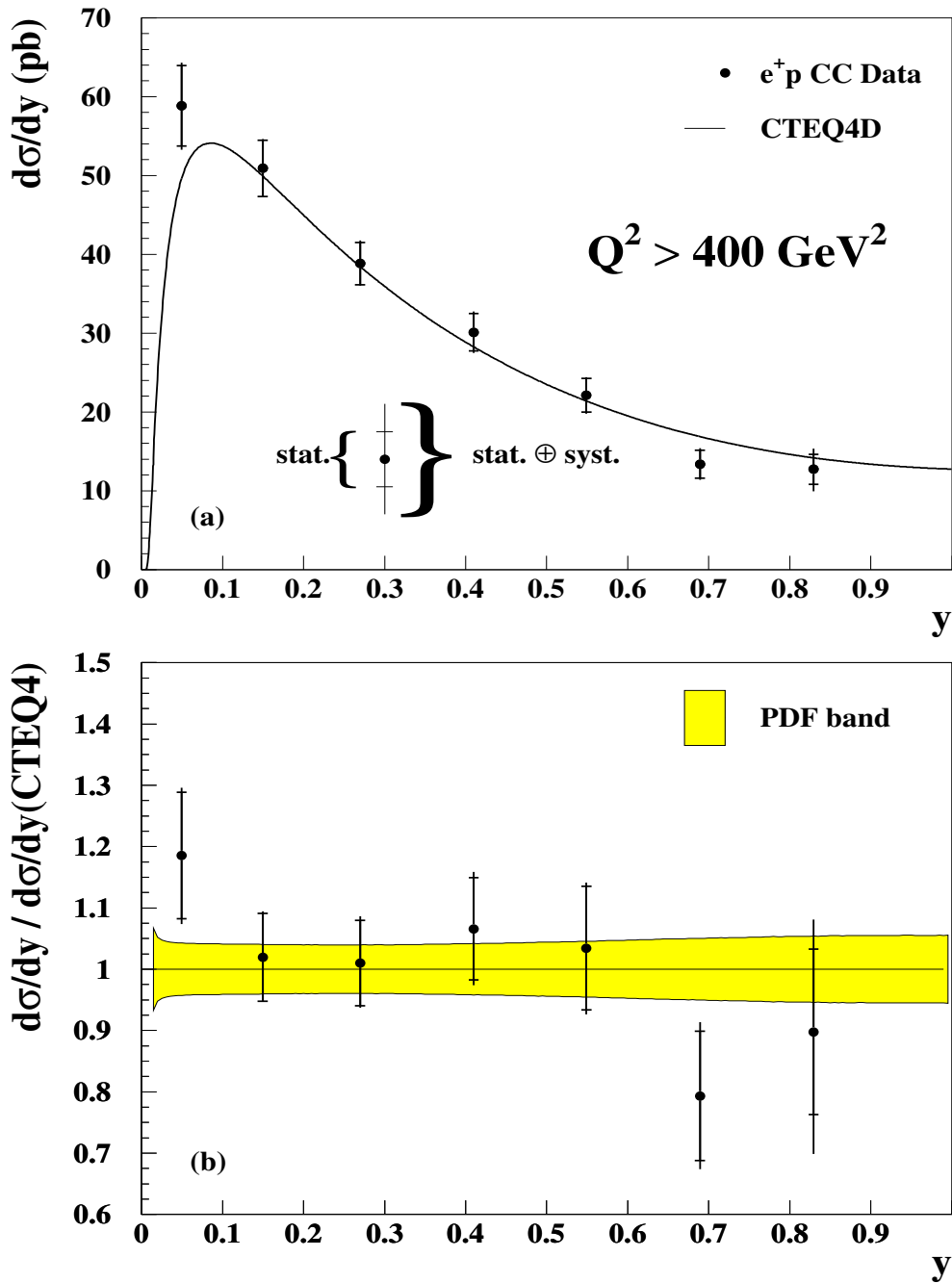


Figure 15: In the top plot, the points with error bars indicate the ZEUS results for the radiatively corrected differential CC e^+p cross-section $d\sigma/dy$. The line is the theoretical prediction. The bottom plot shows the ratio of measured to expected cross-sections, with the shaded band indicating the PDF uncertainty.

Figure 15 may indicate that this excess is related to a y -behavior which is slightly softer than expected. Indeed one may speculate whether these (admittedly not very significant) observations hint to an underestimation of the d distribution at large x , which could both explain the tendencies in the experimental data and be in accordance with recent phenomenological and theoretical work.^{20,21}

The Q^2 dependence of the CC cross-section is proportional to the square of the W propagator (see eq. (10)) and can hence be used to infer the W mass. Although the resulting precision is inferior to that of the Tevatron and LEP results, it constitutes an important check of the SM consistency in the regime of highly virtual, space-like W propagators. The values obtained by H1 ($M_W = 81.2 \pm 3.3$ (stat.) ± 4.3 (syst.) GeV) and by ZEUS ($M_W = 78.6_{-2.4}^{+2.5}$ (stat.) $_{-3.0}^{+3.3}$ (syst.) GeV) are in perfect agreement with the current world average.

Comparison of NC and CC Cross-Sections:

A comparison of $d\sigma/dQ^2$ for NC and CC e^+p reactions as measured by both experiments is shown in Fig. 16. Note that the ZEUS and the H1 results agree well over the full cross-section range of more than five decades. For $Q^2 \gtrsim 10000$ GeV², the NC and the CC differential cross-sections are indeed similar in magnitude and Q^2 -slope, indicating the restoration of full electroweak symmetry at this scale.

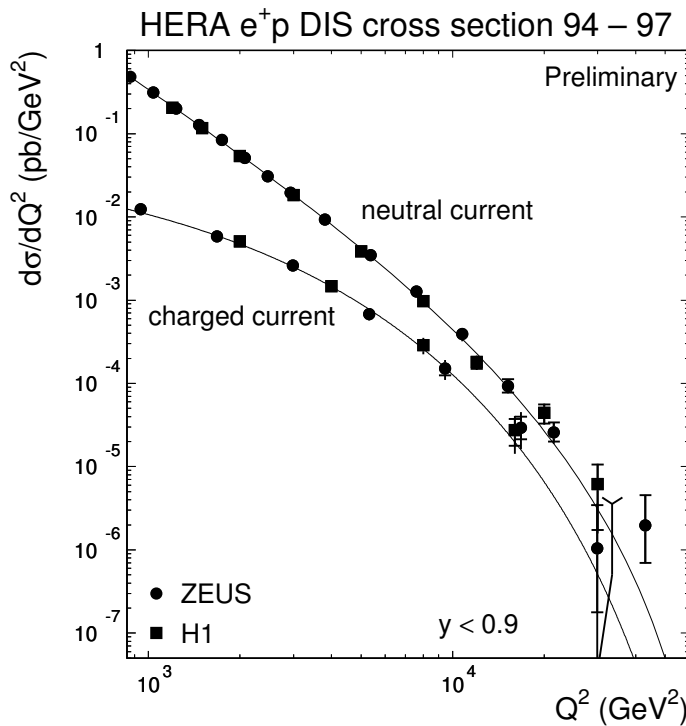


Figure 16: Comparison of the NC and CC cross-sections $d\sigma/dQ^2$ for $y < 0.9$. The circles indicate the ZEUS measurements, the squares those of H1, the lines represent the theoretical predictions. All cross-sections are radiatively corrected.

5 Scenarios Beyond the Standard Model

In this section, we will constrain ourselves to hypothesized processes beyond the SM producing event signatures which are indistinguishable from NC scattering on the event-by-event basis, and which have matrix elements which in fact interfere with the SM ones. There are two such scenarios which have been tested by both collaborations: contact interactions and the on-shell production of a heavy e^+p resonance. We will not consider searches for pair production of supersymmetric MSSM particles, for excited fermions, or for new physics inducing CC-like reactions or final states with muons having high transverse momentum.

Search for Contact Interactions:

A wide class of hypothesized new interactions at characteristic mass scales in the TeV range would modify the differential HERA DIS cross-sections in a way which can be parameterized by effective four-fermion contact interactions (CI) coupling electrons to quarks ($eeqq$), in much the same way as four-fermion interactions were once used to describe weak interactions.

The Lagrangian for a ($eeqq$) CI is given by

$$\begin{aligned}
 \mathcal{L} = \mathcal{L}_{\text{SM}} + \frac{g^2}{\Lambda^2} & \left[\eta_s^q (\bar{e}_L e_R) (\bar{q}_L q_R) + \eta_s^{q'} (\bar{e}_L e_R) (\bar{q}_R q_L) + \text{h.c.} \right. && \text{scalar} \\
 & + \eta_{LL}^q (\bar{e}_L \gamma^\mu e_L) (\bar{q}_L \gamma_\mu q_L) + \eta_{LR}^q (\bar{e}_L \gamma^\mu e_L) (\bar{q}_R \gamma_\mu q_R) \\
 & + \eta_{RL}^q (\bar{e}_R \gamma^\mu e_R) (\bar{q}_L \gamma_\mu q_L) + \eta_{RR}^q (\bar{e}_R \gamma^\mu e_R) (\bar{q}_R \gamma_\mu q_R) && \text{vector} \quad (14) \\
 & \left. + \eta_T^q (\bar{e}_L \sigma^{\mu\nu} e_R) (\bar{q}_L \sigma_{\mu\nu} q_R) + \text{h.c.} \right] , && \text{tensor}
 \end{aligned}$$

where g is the coupling, Λ is the effective mass scale, the η_i^q determine the relative size and sign of the individual terms, and the indices L, R denote the helicity of the respective fermions. ZEUS and H1 only consider the vector terms because strong limits beyond the HERA sensitivity have already been placed on the scalar and on the tensor terms.²² Since g and Λ always enter in the combination g^2/Λ^2 , we use the convention $g^2 = 4\pi$ to relate CI strengths to the corresponding effective mass scales. Furthermore, each of the $\eta_{\alpha\beta}^q$ ($\alpha, \beta = L, R$) is assumed to be either zero or ± 1 , and to be flavor-symmetric (i.e. $\eta^d = \eta^s = \eta^b$ and $\eta^u = \eta^c = \eta^t$).

Different patterns of the $\eta_{\alpha\beta}^q$ define different CI scenarios, corresponding to distinct physics models. The CI scenarios considered in the HERA analyses are

CI	η_{LL}^u	η_{LR}^u	η_{RL}^u	η_{RR}^u	η_{LL}^d	η_{LR}^d	η_{RL}^d	η_{RR}^d	studied by
VV	+	+	+	+	+	+	+	+	ZEUS, H1
AA	+	-	-	+	+	-	-	+	
VA	+	-	+	-	+	-	+	-	
X1	+	-	0	0	+	-	0	0	ZEUS
X2	+	0	+	0	+	0	+	0	
X3	+	0	0	+	+	0	0	+	
X4	0	+	+	0	0	+	+	0	
X5	0	+	0	+	0	+	0	+	
X6	0	0	+	-	0	0	+	-	
U1	+	-	0	0	0	0	0	0	ZEUS
U4	0	+	+	0	0	0	0	0	
U5	0	+	0	+	0	0	0	0	
LL	+	0	0	0	+	0	0	0	H1
LR	0	+	0	0	0	+	0	0	
RL	0	0	+	0	0	0	+	0	
RR	0	0	0	+	0	0	0	+	

Table 1: *CI scenarios studied by ZEUS and H1. Each line describes two different η patterns, corresponding to an overall sign +1 or -1.*

summarized in Tab. 1. Except the purely chiral terms, all scenarios obey $\eta_{LL}^q + \eta_{LR}^q - \eta_{RL}^q - \eta_{RR}^q = 0$ in order to avoid strong CI limits²³⁻²⁵ implied by recent measurements of parity-violating transition amplitudes in cesium atoms.²⁶

The cross-section modification in presence of CI affects mainly $d\sigma/dQ^2$, which acquires two extra terms: one proportional to $\pm Q^2/\Lambda^2$ (from the SM-CI interference), and one proportional to $+Q^4/\Lambda^4$ (pure CI). In order to search for such signatures, ZEUS¹⁰ used log-likelihood techniques based on the comparison of the measured Q^2 and (x, y) distributions to the corresponding Monte Carlo (MC) simulations, in which CIs were taken into account by reweighting the events. No significant indications for CIs were found. One-sided 95% C.L. lower limits on Λ were set using MC techniques. H1 performed a χ^2 -fit of the predicted to the measured $d\sigma/dQ^2$ and inferred two-sided 95% C.L. limits from the resulting changes in χ^2 with respect to the fit to the SM, which describes the data well.

In Tab. 2, the Λ limits are summarized and compared to corresponding results recently reported by CDF²⁷ ($q\bar{q} \rightarrow e^+e^-$) and the LEP experiments²⁸⁻³⁰ ($e^+e^- \rightarrow q\bar{q}$), and to the limits derived from the atomic parity violation results (see ref. 24 and references therein). All LEP and CDF limits except those for for the U4

Type	95% C.L. lower limits on Λ [TeV]						
	ZEUS,H1		CDF	OPAL,ALEPH,L3			APV (u/d)
	ref. 10	ref. 11	ref. 27	ref. 28	ref. 29	ref. 30	ref. 24
VV+	4.9	4.5	3.5	4.1	6.7	3.2	—
VV-	4.6	2.5	5.2	5.7	7.4	3.9	—
AA+	2.0	2.0	3.8	6.3	7.4	4.3	—
AA-	4.0	3.8	4.8	3.8	8.2	2.9	—
VA+	2.8	2.6	—	—	—	—	—
VA-	2.8	2.8	—	—	—	—	—
X1+	1.8	—	—	—	—	—	—
X1-	3.0	—	—	—	—	—	—
X2+	3.9	—	—	—	—	—	—
X2-	1.9	—	—	—	—	—	—
X3+	2.8	—	—	4.4	6.9	3.2	—
X3-	1.5	—	—	3.8	7.7	2.8	—
X4+	4.5	—	—	3.1	2.9	2.4	—
X4-	4.1	—	—	5.5	4.5	3.7	—
X5+	3.8	—	—	—	—	—	—
X5-	3.0	—	—	—	—	—	—
X6+	3.0	—	—	—	—	—	—
X6-	1.9	—	—	—	—	—	—
U1+	2.9	—	—	—	—	—	—
U1-	1.6	—	—	—	—	—	—
U4+	4.4	—	2.3	—	—	1.8	—
U4-	4.6	—	3.2	—	—	2.2	—
U5+	3.6	—	—	—	—	—	—
U5-	4.2	—	—	—	—	—	—
LL+	—	2.4	2.5	4.4	5.6	3.0	7.4/7.9
LL-	—	1.2	3.7	2.8	6.4	2.1	11.7/12.3
LR+	—	3.0	2.8	3.3	3.0	2.4	7.4/7.9
LR-	—	1.5	3.3	3.6	3.2	2.6	11.7/12.3
RL+	—	3.0	2.9	2.5	2.3	2.0	11.7/12.3
RL-	—	1.6	3.2	4.9	4.0	3.2	7.4/7.9
RR+	—	2.4	2.6	3.0	4.1	2.3	11.7/12.3
RR-	—	1.2	3.6	3.9	4.5	2.7	7.9/7.4

Table 2: Lower limits on Λ at 95% C.L. from the HERA experiments, compared to corresponding limits reported recently by CDF and by the LEP experiments, and to limits derived from measurements of parity-violating atomic transitions. The ZEUS, H1 and ALEPH results are preliminary.

scenario assume flavor-symmetry. The HERA and the other experiments are all sensitive to CI at mass scales of a few TeV. Limits for the X1, X2, X5, X6, U1 and U5 scenarios are derived only by ZEUS. The relative sensitivity to different CI scenarios depends on the SM-CI interference sign which is opposite for e^+p and for e^+e^- and $p\bar{p}$ reactions. Where available, the CERN limits mostly exceed those of HERA and CDF. However, this conclusion depends on the assumption of flavor-symmetric CI; CI coupling e.g. only to the first-generation quarks would give almost the same results for ep or $p\bar{p}$ scattering but significantly different limits in the case of LEP.

Search for e^+p resonance production:

The HERA kinematic range allows to access eq reactions at a center-of-mass energy of 200 GeV and beyond, where new particles coupling to electrons and quarks (leptoquarks, LQ) might be resonantly produced. If the LQ decayed back to eq , the events would be NC-like. The experimental signature would be a peak in $M = \sqrt{xs}$ and a y distribution which is either flat (scalar LQ) or proportional to $(1-y)^2$ (vector LQ). The LQ cross-section depends on the LQ- e - q coupling (λ), on the LQ mass (M_{LQ}), and on the branching ratio of the decay $LQ \rightarrow eq$ (β). Generally, two types of LQ's are distinguished: (i) the "classical" LQ's³¹ which only couple to eq or $\nu q'$ and have $\beta = 0, 0.5$ or 1 ; (ii) squarks in R_P -violating extensions of Supersymmetry, which have additional R_P -conserving decay modes and therefore can have $\beta \ll 1$ (for details see e.g. ref. 32). The type-(ii) LQ's avoid the mass limits of the DØ collaboration at the Tevatron who have searched for LQ pair production and exclude at 95% C.L. scalar³³/vector³⁴ LQ's with $M_{LQ} < 225/298$ GeV ($M_{LQ} < 204/270$ GeV) for $\beta = 1$ ($\beta = 0.5$).^f

Both ZEUS⁸ and H1^{9,36} have reported searches for LQ signals. Figure 17 shows the M -distribution of H1, for two different cuts in y_e . The excess of events around $x = 0.45$ seen in Fig. 11 is again evident at $M \approx 200$ GeV. From the comparison of the measured and expected M distributions, H1 sets limits on β as a function of M_{LQ} for fixed values of λ . As can be seen from Fig. 18, the HERA experiments still have a discovery window for a LQ with $\beta \lesssim 0.3$ and $M_{LQ} \gtrsim 200$ GeV.

The M distribution as measured by ZEUS⁸ is shown in Fig. 19. Again, some

^f A recent combined analysis³⁵ of the CDF and DØ data yields a mass limit of $M_{LQ} > 242$ GeV for scalar LQ's with $\beta = 1$.

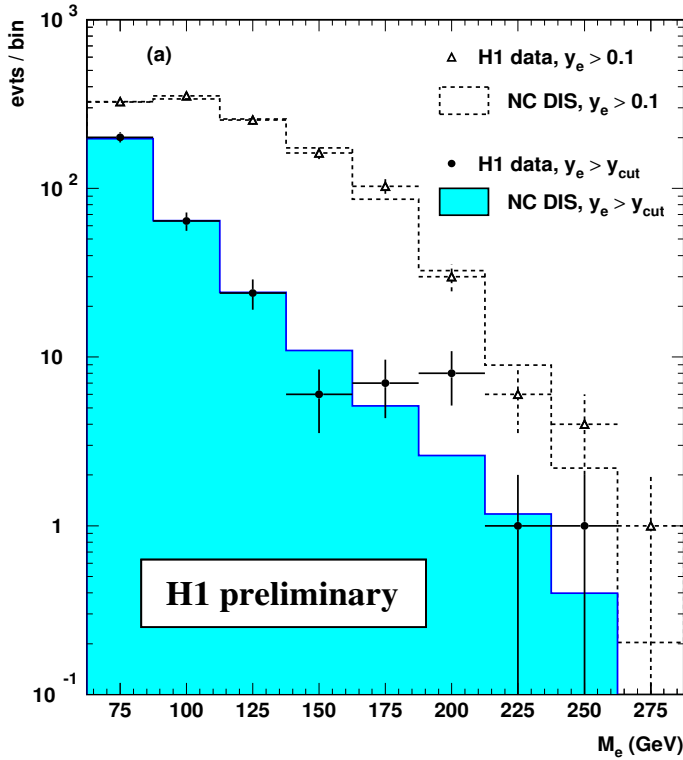


Figure 17: Distributions of M from H1 for two different cuts on y_e (error bars). The dashed (solid) histograms represent the expected distributions for $y_e > 0.1$ ($y_e > y_{\text{cut}}$, where y_{cut} is a function of M).

H1 Preliminary

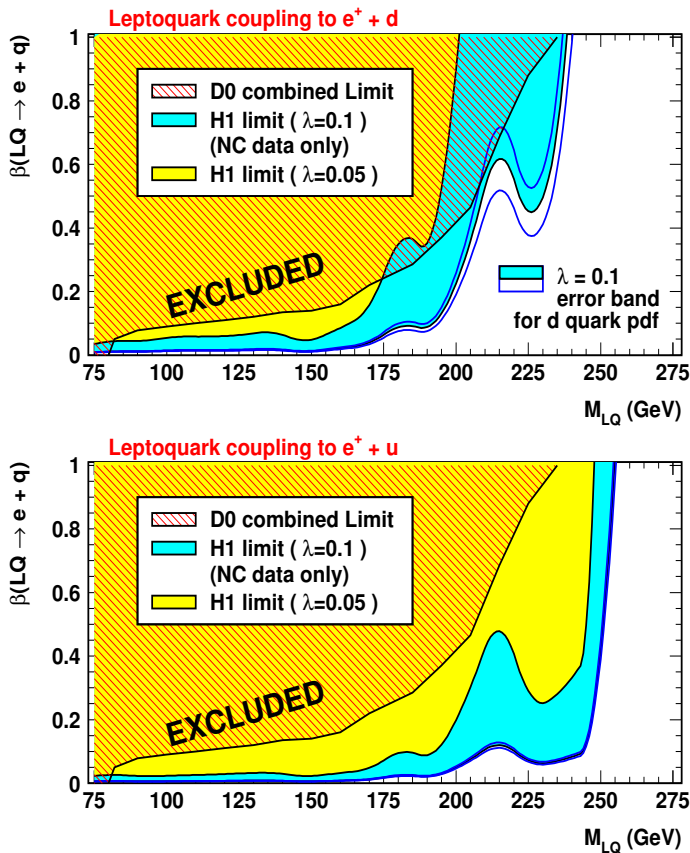


Figure 18: Limits on LQ production from H1, for LQ's coupling to e^+d (top) and to e^+u (bottom). For different assumptions on the coupling λ , the shaded regions indicate as a function of M_{LQ} the values of the branching ratio β which are excluded at 95% C.L. The $D\bar{D}$ exclusion limits are marked by the hatched area.

ZEUS 1994-97 Preliminary

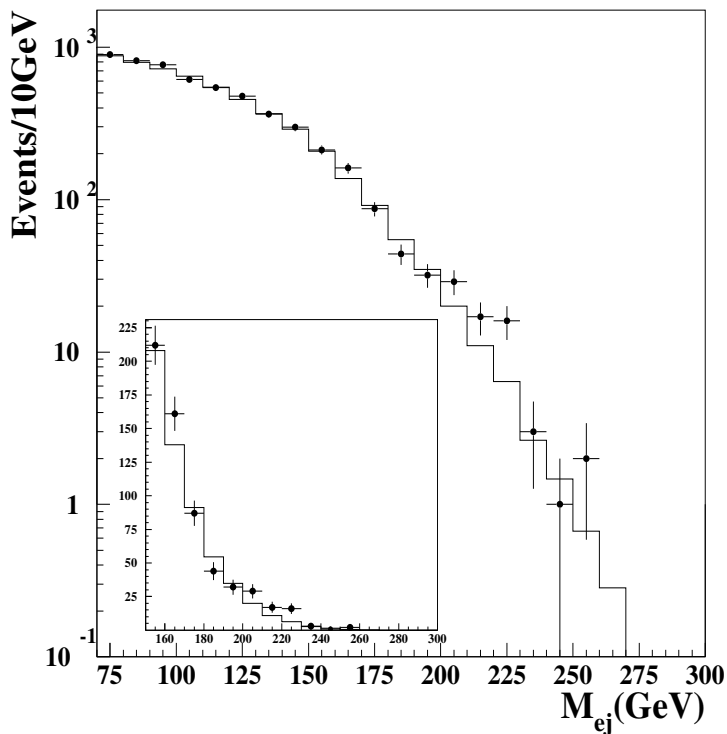


Figure 19: *Distribution of M measured by ZEUS (points with error bars). The histogram represents the expected distribution. The insert plot shows the same distributions with a linear vertical scale.*

ZEUS 1994-97 Preliminary

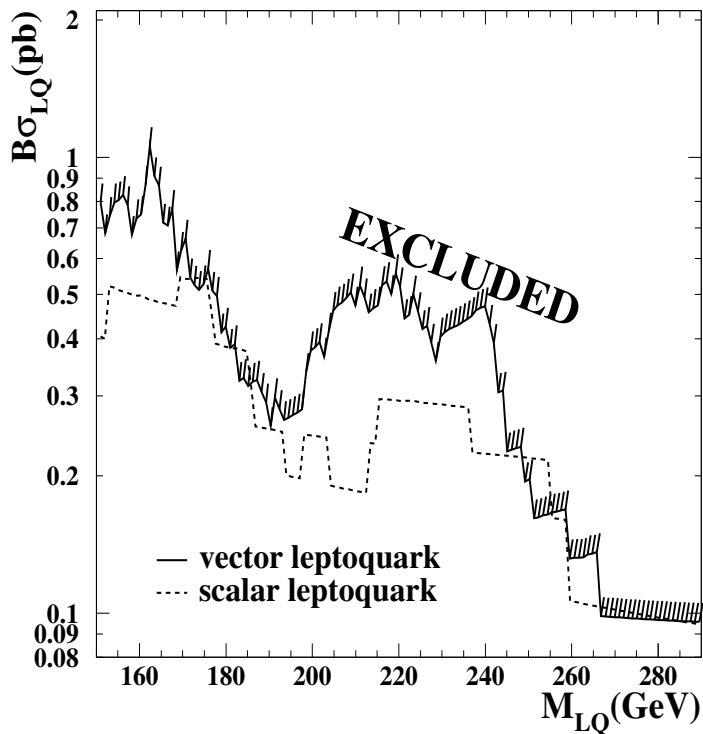


Figure 20: *95% C.L. limits on the product of LQ production cross-section and β (here denoted B) reported by ZEUS. The solid (dashed) histogram indicate the borders of the excluded regions for vector (scalar) LQ's as function of M_{LQ} .*

excess around $M \approx 220$ GeV is visible. However, the kinematic properties of the events in this region do not exhibit significant indications for LQ production, and ZEUS hence sets limits on the corresponding cross-section $\sigma(e^+p \rightarrow \text{LQ})$. The 95% C.L. limit on $\beta \cdot \sigma(e^+p \rightarrow \text{LQ})$ resulting from a comparison of the measured and the predicted M distributions is displayed in Fig. 20.

6 Conclusion and Outlook

The HERA experiments ZEUS and H1 have both collected a total of approximately 40 pb^{-1} of e^+p collision data in the years 1994–1997. These data allow for the first time to study deep-inelastic scattering in the region of high Q^2 above several 100 GeV with good statistical precision.

Particular interest in e^+p scattering at $Q^2 \gtrsim 15000 \text{ GeV}^2$ was stimulated in early 1997, when both experiments reported an excess of events in their 1994–1996 data samples above the expectations in this kinematic regime. Meanwhile the data samples have about doubled, and careful measurements of the high- Q^2 differential cross-sections, both for NC and for CC reactions are available. Very good agreement between measured and expected cross-sections is generally observed, with the possible exception of the highest x and Q^2 intervals, where the data are above the prediction. The data allow for the first time to observe the restoration of full electroweak symmetry at a scale of $Q^2 \sim M_W^2, M_Z^2$.

It has been hypothesized in a series of papers that the excess at high Q^2 may be a first glimpse at new physics beyond the Standard Model. Dedicated searches for signatures of different such scenarios have been performed. No evidence for new processes has been found, and new limits on contact interactions and positron-quark resonance production are reported. It remains to be studied with increased data statistics whether the observed excess is a statistical fluctuation or a sign of something new.

Currently HERA is operated with electrons (e^-), and these data together with the existing e^+p sets will allow a detailed study of high- Q^2 structure functions and parton distributions and will help to reduce the uncertainties of the theoretical cross-section predictions. In a shutdown of about nine months in 1999/2000, HERA will be upgraded to deliver significantly higher luminosity and also longitudinally polarized e beams to the experiments. From 2001 onwards, the e

polarization and the expected integrated luminosities of more than 100 pb^{-1} per experiment and year will allow to study the region of highest Q^2 with yet much higher precision and with an additional degree of freedom. We await with excitement the measurements and possible discoveries which will be made possible by these data.

Acknowledgments. None of the research reported here would have been possible without the dedicated efforts of the HERA machine physicists and technicians, and of all those who contributed to the design, construction, maintenance and operation of the detectors. I'm indebted to Martin Erdmann and Stefan Schlenstedt for the careful reading of the manuscript. Last but not least, I would like to thank the organizers of the SLAC Topical Conference for a very inspiring meeting and a pleasant stay in California.

References

- [1] H1 Coll., I.Abt et al., Report DESY-93-103, DESY (1993);
H1 Coll., I.Abt et al., Nucl. Instrum. Methods **A 386** (1997) 310.
- [2] ZEUS Coll., ed. U. Holm, Status Report, 1993.
- [3] ZEUS Coll., J.Breitweg et al., Z. Phys. **C 74** (1997) 207.
- [4] H1 Coll., C.Adloff et al., Z. Phys. **C 74** (1997) 191.
- [5] ZEUS Coll., Subm. paper 753 to ICHEP98, Vancouver, July 23-29, 1998.
- [6] ZEUS Coll., Subm. paper 751 to ICHEP98, Vancouver, July 23-29, 1998.
- [7] H1 Coll., Subm. paper 533 to ICHEP98, Vancouver, July 23-29, 1998.
- [8] ZEUS Coll., Subm. paper 754 to ICHEP98, Vancouver, July 23-29, 1998.
- [9] H1 Coll., Subm. paper 579 to ICHEP98, Vancouver, July 23-29, 1998.
- [10] ZEUS Coll., Subm. paper 753 to ICHEP98, Vancouver, July 23-29, 1998.
- [11] H1 Coll., Subm. paper 584 to ICHEP98, Vancouver, July 23-29, 1998.
- [12] G.Bernardi, Contribution to these proceedings.
- [13] V.N.Gribov, L.N.Lipatov, Sov. J. Nucl. Phys. **15** (1972) 438;
L.N.Lipatov, Yad. Fiz. **20** (1974) 181, Sov. J. Nucl. Phys **20** (1975) 94;
G.Altarelli, G.Parisi, Nucl. Phys. **B 126** (1977) 298;
Yu.L.Dokshitser, Sov. Phys. JETP **46** (1977) 641.

- [14] A.D.Martin, et al., Eur. Phys. J. **C 4** (1998) 463.
- [15] CTEQ Coll., H.L.Lai et al., Phys. Rev. **D 55** (1997) 1280.
- [16] M.Glück, E.Reya, A.Vogt, Z. Phys. **C 67** (1995) 433.
- [17] M.A.J.Botje, Preprint NIKHEF-97-028, NIKHEF (1997), hep-ph/9707289.
- [18] B.Straub, for the ZEUS and H1 Collaborations, in *Proc. 18th Int. Symp. on Lepton-Photon Interactions (LP97), Hamburg, 1997*, p. 3.
- [19] A.D.Martin, W.J.Stirling, R.G.Roberts, Preprint DTP 93-86/RAL-93-077, Univ. Durham/Rutherford Lab. (1993).
- [20] W.Melnitchouk, A.Thomas, Acta Phys. Pol. **B 27** (1996) 1407;
W.Melnitchouk, A.W.Thomas, Phys. Lett. **B 377** (1996) 11;
W.Melnitchouk, J.C.Peng, Phys. Lett. **B 400** (1997) 220.
- [21] U.K.Yang, A.Bodek, Q.Fan, Preprint UR-1519, Univ. Rochester (1998), hep-ph/9806457.
- [22] P.Haberl, F.Schrempp, H.U.Martyn, in *Proc. Workshop Physics at HERA*, ed. W.Buchmüller, G.Ingelman, Hamburg, Germany, 1991, p. 1133.
- [23] V.Barger et al., Phys. Rev. **D 57** (1998) 391.
- [24] A.Deandrea, Phys. Lett. **B 409** (1997) 277.
- [25] L.Giusti, A.Strumia, Phys. Lett. **B 410** (1997) 229.
- [26] C.S.Wood et al., Science **275** (1997) 1759.
- [27] CDF Coll., F.Abe et al., Phys. Rev. Lett. **79** (1997) 2198.
- [28] OPAL Coll., G.Abbiendi et al., Eur. Phys. J. **C 6** (1999) 1.
- [29] ALEPH Coll., ALEPH 98-060/CONF 98-031, subm. paper 906 to ICHEP98, Vancouver, July 23-29, 1998.
- [30] L3 Coll., M.Acciarri et al., Phys. Lett. **B 433** (1998) 163.
- [31] W.Buchmüller, R.Rückl, D.Wyler, Phys. Lett. **191 B** (1987) 442.
- [32] G.Altarelli et al., Nucl. Phys. **B 506** (1997) 3.
- [33] DØ Coll., B.Abbott et al., Phys. Rev. Lett. **80** (1998) 2051.
- [34] J.A.Valls, in *Proc. 32. Recontres de Moriond: QCD and High-Energy Hadronic Interactions, Les Arcs, France, 1997*.
- [35] CDF and DØ Coll., C.Grosso-Pilcher et al., hep-ex/9810015, 1998.
- [36] H1 Coll., Subm. paper 580 to ICHEP98, Vancouver, July 23-29, 1998.